Adhesion and friction between a smooth elastic spherical asperity and a plane surface

By K. L. Johnson

Cambridge University, 1 New Square, Cambridge CB1 1EY, UK

Attempts to establish the relationship between adhesion and friction at the contact of solid surfaces has been frustrated by their inevitable roughness. The recent development of *nanotribology*, in which a single asperity contact can be modelled in the surface force apparatus (SFA) or the atomic force microscope (AFM), has made possible the simultaneous measurement of friction and adhesion in a sliding experiment. For the case of pure adhesion, continuum mechanics models exist which assist in the interpretation of the measurements. In this paper these models are extended to include both static and sliding friction. The approach is through the concept of fracture mechanics, in which the rate of release of elastic strain energy is equated to the work done against surface forces, both frictional and adhesive. The model appears to be consistent with currently available experimental data.

1. Introduction

The idea that friction is associated with adhesion is an old one, generally attributed to Desaguliers in the early years of the 18th century, but it was Bowden & Tabor (1950) who made it a leading concept in their 'plastic junction' theory of friction. The difficulty in providing experimental support for this or any other theory of friction lies in the inevitable roughness of real surfaces and the fact that the *real* area of contact is not known. Further, adhesion is difficult to measure since elastic relaxation of the higher asperities when the load is removed breaks the adhesive contact of the lower junctions. To avoid these difficulties attempts are made to experiment with a single asperity contact, usually modelled by a spherical tip in contact with a plane surface, in which the real and apparent areas of contact coincide. This quest has been significantly advanced in recent years by the development of two novel instruments: (i) the surface force apparatus (SFA), in which crossed cylinders of cleaved mica or similar surfaces are pressed together (Homola *et al.* 1990); and (ii) the atomic force microscope (AFM) in which a probe of tip radius 10–100 nm makes contact with a flat surface (Sarid 1991). Both instruments have been developed to permit sliding motion and to measure both normal and tangential (friction) forces, which enables the interaction between adhesion and friction to be observed directly. A different situation in which perfect contact can be attained arises when one or both solids are of a compliant material, such as rubber, polymer or gelatine, which can conform elastically to small irregularities of the surfaces.

Bowden & Tabors' plastic-junction theory was originally developed with ductile metals in mind where, as the name implies, the contacting asperities were assumed to deform plastically. In the intervening years, with highly finished or well run-in

Proc. R. Soc. Lond. A (1997) **453**, 163–179
Printed in Great Britain

TEX Paper

surfaces, or with either harder or more compliant materials, the *elastic* deformation of asperities has been recognized to play a more significant role. AFM experiments in ultra-high vacuum frequently result in plastic deformation. This presents an important problem in nanomechanics, but the present work, like the adhesion theories of which it is an extension, will be restricted to perfectly elastic deformation. Single asperity contact will be modelled by a spherical tip in contact with a flat. The aim is to derive a continuum mechanics model of the static and sliding friction of such a contact in the presence of adhesive forces. The AFM is capable of resolving variations of sliding friction force at the periodicity of individual atoms. It will be appreciated, however, that a continuum theory will 'smear out' periodic variations on the atomic scale.

Continuum theories for the adhesion and separation of a spherical elastic contact under the action of purely normal forces are well advanced. Adhesion between *rigid* spheres where the surface forces are governed by the Lennard–Jones potential was analysed by Bradley (1932). Corresponding theories taking elastic deformation into account were presented by Johnson, Kendall & Roberts (JKR) in 1971 and by Derjaguin, Muller & Topolov (DMT) in 1975 (subsequently shown to be in error by Muller *et al.* (1983) and by Pashley (1984)). These theories, at first thought to be competitive, were recognized to apply to the opposite ends of a spectrum of a non-dimensional parameter:

$$\mu = \left(\frac{Rw^2}{E^{*2} z_0^3} \right)^{1/3}, \tag{1.1}$$

where the R is the radius of the spherical surface, w is the 'work of adhesion' (equals twice the surface energy γ), z_0 is the equilibrium spacing in the Lennard–Jones potential and E^* is the combined elastic modulus $= [(1-\nu_1^2)/E_1 + (1-\nu_2^2)/E_2]^{-1}$. The parameter μ was shown by Tabor (1977) to be a measure of the magnitude of the elastic deformation compared with the range of surface forces. For μ small (less than 0.1 say) elastic deformation is negligible and the Bradley analysis provides a good approximation; for μ large (greater than 5 say) the JKR theory is good. For intermediate values of μ numerical analysis is necessary to match the elastic deformation to the force-separation relationship. This was first done (for a Lennard–Jones potential) by Muller *et al.* (1980); more complete computations have recently been made by Greenwood (1996).

A useful analysis in closed form of the intermediate regime has been made by Maugis (1992) using the Dugdale approximation that the adhesive force intensity σ_0 is constant until a separation h_0 is reached, whereupon it falls to zero (see figure 1). For the work of adhesion w and the maximum force σ_0 to match those of Lennard–Jones, $h_0 = 0.971 z_0$. For analytical convenience this analysis will be used to model adhesion in the present paper. It will be outlined in principle in the next section and the relevant results quoted. It will also be shown that when Tabor's elasticity parameter μ is small (less than 5 say), the Maugis–Dugdale relationships reduce to the well known JKR equations.

The effect of adhesive forces in the contact of spheres is to increase the contact radius above that prescribed by the Hertz theory. When tangential forces are applied to such an adhesive contact the consequences are not at all well understood. There is some experimental evidence (see, for example, Savkoor & Briggs 1977) that the surfaces tend to peel apart, showing that there is some interaction between normal

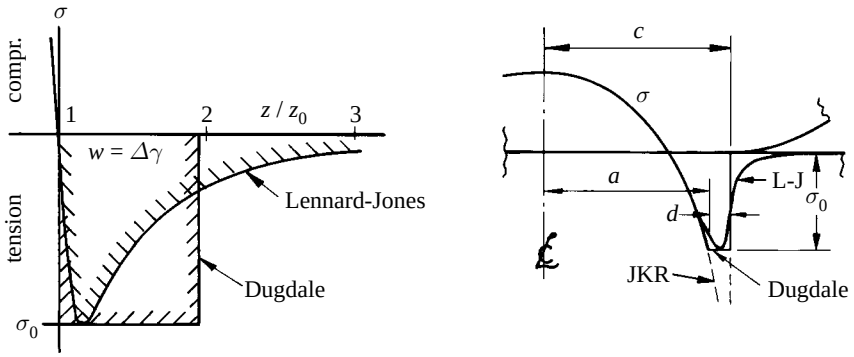

Figure 1. (*a*) Force–separation laws: Lennard–Jones, Dugdale; (*b*) traction distributions.

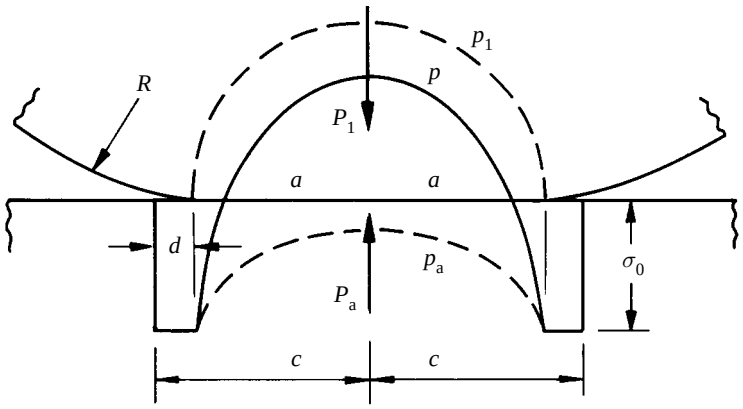

Figure 2. The Maugis–Dugdale distribution of surface traction comprises two terms: the Hertz pressure p_1 (equation (2.1)) acting on area radius a and the adhesive tension p_a (equation (2.6)) acting on area radius c.

and tangential surface forces. This aspect of the problem will be considered and incorporated in the continuum model in § 4.

2. Continuum theories of adhesion

(*a*) *The Maugis–Dugdale theory*

The circular contact between a sphere of radius R and a flat surface, as described by the Maugis–Dugdale theory, is shown in figure 2. Intimate contact is maintained over a central region of radius a; adhesive forces of intensity σ_0 extend to a radius c. In the annulus $a < r < c$ the surfaces separate slightly by a distance increasing from zero to h_0. The distribution of surface traction comprises the following two terms.

(i) The Hertz pressure associated with a contact of radius a is given by

$$p_1(r) = (3P_1/2\pi a^2)\{1 - (r/a)^2\}^{1/2}, \tag{2.1}$$

where

$$P_1 = 4E^* a^3/3R, \tag{2.2}$$

the elastic compression by

$$\delta_1 = u_{z1}(0) = a^2/R, \tag{2.3}$$

the displacement at $r = c$ by

$$u_{z1}(c) = (1/\pi R)\{(2a^2 - c^2)\sin^{-1}(a/c) + a\sqrt{c^2 - a^2}\} \tag{2.4}$$

and the gap between the surfaces by

$$h_1(c) = c^2/2R - \delta_1 + u_{z1}(c). \tag{2.5}$$

(ii) The adhesive (Dugdale) stress is given by

$$\begin{aligned} p_{\mathrm{a}}(r) &= -(\sigma_0/\pi)\arccos\left\{\frac{2a^2 - c^2 - r^2}{c^2 - r^2}\right\}, \quad r \leqslant a, \\ &= -\sigma_0, \quad a \leqslant r \leqslant c, \end{aligned} \tag{2.6}$$

the adhesive force by

$$P_{\mathrm{a}} = -2\sigma_0\{c^2\arccos(a/c) + a\sqrt{c^2 - a^2}\}, \tag{2.7}$$

the compression by

$$\delta_{\mathrm{a}} = -(2\sigma_0/E^*)\sqrt{c^2 - a^2}, \tag{2.8}$$

and the gap between the surfaces at $r = c$ by

$$h_{\mathrm{a}}(c) = (4\sigma_0/\pi E^*)\{\sqrt{c^2 - a^2}\arccos(a/c) + a - c\}. \tag{2.9}$$

The net traction acting on the contact area $p(r)$ is the sum of $p_1(r)$ and $p_{\mathrm{a}}(r)$, given by equations (2.1) and (2.6), as shown in figure 2. Similarly, the net contact force $P = P_1 + P_{\mathrm{a}}$. The adhesive traction for the Dugdale model falls to zero when the separation of the surfaces exceeds h_0. Therefore we may write

$$h(c) = h_1(c) + h_{\mathrm{a}}(c) = h_0 = w/\sigma_0. \tag{2.10}$$

We now introduce the non-dimensional parameters:

$$\bar{a} \equiv a\left(\frac{4E^*}{3\pi wR^2}\right)^{1/3}, \quad \bar{c} \equiv c\left(\frac{4E^*}{3\pi wR^2}\right)^{1/3}, \quad \bar{A} \equiv \pi\bar{c}^2,$$

$$\bar{P} \equiv \frac{P}{\pi wR}, \quad \bar{\delta} \equiv \delta\left(\frac{16E^{*2}}{9\bar{u}^2w^2R}\right)^{1/3},$$

and

$$\lambda \equiv 2\sigma_0\left(\frac{9R}{16\pi wE^{*2}}\right)^{1/3}. \tag{2.11}$$

It may be shown that $\lambda = 1.16\mu$. It is thus an alternative measure of the ratio of the elastic deformation to the range of surface forces. Substituting for $h_1(c)$ and $h_{\mathrm{a}}(c)$ from equations (2.5) and (2.9), and making use of the above non-dimensional parameters, equation (2.10) may be written

$$\tfrac{1}{2}\lambda\bar{a}^2\{(m^2 - 2)\arccos(1/m) + \sqrt{m^2 - 1}\} + \tfrac{4}{3}\lambda^2\bar{a}\{\sqrt{m^2 - 1}\arccos(1/m) - m + 1\} = 1, \tag{2.12}$$

where $m = c/a$. From equations (2.2) and (2.7) the net contact force becomes

$$\bar{P} = \bar{P}_1 + \bar{P}_{\mathrm{a}} = \bar{a}^3 - \lambda\bar{a}^2\{\sqrt{m^2 - 1} + m^2\arccos(1/m)\}, \tag{2.13}$$

and, from equations (2.3) and (2.8), the total elastic compression becomes

$$\Delta = \bar{a}^2 - \tfrac{4}{3}\lambda\bar{a}\sqrt{m^2 - 1}. \tag{2.14}$$

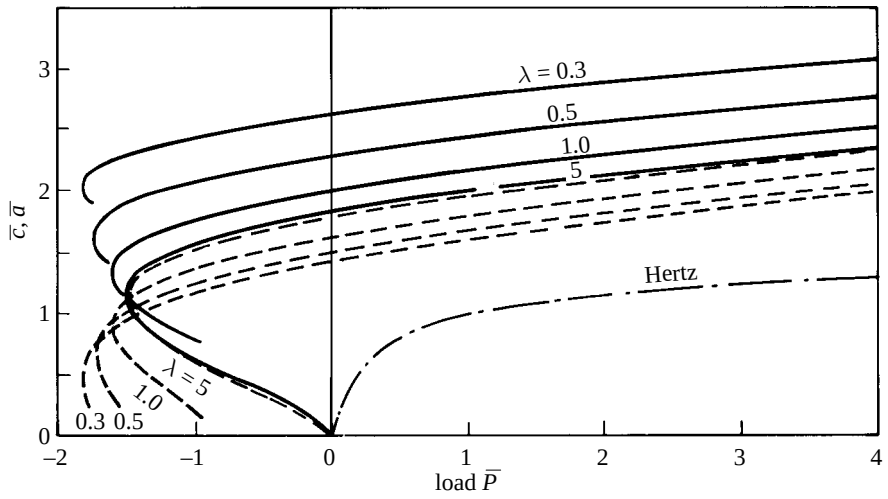

Figure 3. Contact radius–load curves given by the Maugis–Dugdale theory in terms of the parameter λ: – – –, $\bar{a}$; ——, $\bar{c}$. When $\lambda > 5$, $\bar{c} \to \bar{a} \to$ the JKR result.

The variation of $\bar{c}$ and $\bar{a}$ with the load $\bar{P}$, for any particular value of λ, is found by the simultaneous solution of equations (2.12) and (2.13), as shown in figure 3. The effect of adhesion is to increase the contact size (both $\bar{c}$ and $\bar{a}$) above the Hertz value. The surfaces remain in contact at zero load and a negative (tensile) force P_c—the 'pull-off force'—is required to separate them. When λ is large (greater than 5 say) the values of $\bar{c}$ and $\bar{a}$ approach equality and are given by the JKR relationship, as shown later.

(*b*) *The JKR theory*

As the parameter λ is increased, elastic deformation increases the radius a compared with the length d of the 'Dugdale zone' in which the adhesive forces act (see figure 1), i.e.

$$\varepsilon \equiv d/a = (c-a)/a = (m-1) \to 0.$$

Letting $(m-1)$ become small in equation (2.12) gives

$$\tfrac{1}{2}\lambda\bar{a}^2\{\sqrt{2\varepsilon} - \sqrt{2\varepsilon}\} + \tfrac{4}{3}\lambda^2\bar{a}\{\sqrt{2\varepsilon}\cdot\sqrt{2\varepsilon} - \varepsilon\} = 1$$

i.e.

$$\lambda = \sqrt{3/(4\bar{a}\varepsilon)},$$

whereupon equation (2.13) becomes

$$\bar{P} = \bar{a}^3 - \sqrt{3/(4\bar{a}\varepsilon)}\bar{a}^2\{\sqrt{2\varepsilon} + \sqrt{2\varepsilon}\},$$

i.e.

$$\bar{P} = \bar{a}^3 - \sqrt{6\bar{a}^3} = \bar{P}_1 - \sqrt{6\bar{P}_1}. \tag{2.15}$$

The adhesive traction, given by equation (2.6), in the limit becomes

$$p_a(r) = (P/2\pi a^2)\{1-(r/a)^2\}^{-1/2}. \tag{2.16}$$

This traction exhibits infinite tension at the edge of contact ($r = a$), as shown in figure 1*b*, which corresponds to an external axisymmetric crack having a mode I

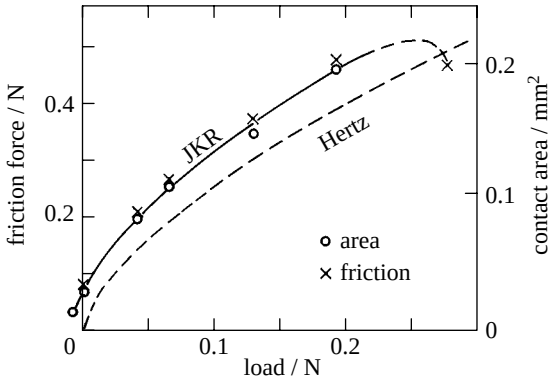

Figure 4. Contact area and friction measurements in dry air between crossed cylinders of smooth mica in the SFA (Homula *et al.* 1992). The variation of both contact area and friction with load fits the JKR theory, giving a uniform frictional stress $\tau_0 = 2 \times 10^7$ N m^{-2}.

stress intensity factor (Maugis & Barquins 1978):

$$K_{\mathrm{I}} = \frac{P}{2a\sqrt{\pi a}} \tag{2.17}$$

3. Static and sliding friction

We now consider an elastic sphere in contact with a flat surface, subjected to a constant normal load P and a monotonically increasing tangential force T. Adhesion forces discussed previously are neglected in this section. The load P gives rise to a circular contact of radius b given by the Hertz theory. If slip at the interface were prevented, the tangential traction at the contact surface ($r \leqslant c$) is given by Johnson (1985)

$$q(r) = (T/2\pi b^2)\{1 - (r/b)^2\}^{-1/2}. \tag{3.1}$$

The singularity at $r = b$ gives rise to mode II and mode III stress intensity factors around the periphery given by

$$K_{\mathrm{II}} = \frac{T}{2b\sqrt{\pi b}} \cos\vartheta \quad \text{and} \quad K_{\mathrm{III}} = \frac{T}{2b\sqrt{\pi b}} \sin\vartheta, \tag{3.2}$$

where ϑ is the angle between the radius vector at the point in question and the direction of T.

If we were dealing with the conventional mode II fracture of a solid containing an external axisymmetric crack, when K_{II} or K_{III} reach critical values the neck would shear in an unstable manner. But the contact situation is different. As the stress intensity is relieved by interfacial microslip, which penetrates into the contact area from the periphery, the 'crack faces' behind the 'crack front' remain pressed into contact by the Hertz pressure. This situation has been examined in the past by Savkoor (1987), but recent experimental evidence suggests a somewhat different approach. In dry sliding experiments of mica on mica, by Homola *et al.* (1990) in the SFA, friction and contact area were measured simultaneously and found to be in direct proportion (figure 4), showing that the frictional shear stress was constant, independent of load. Similar experiments in the AFM by Carpick *et al.* (1996), although unable to measure the contact area directly, found that the friction measurements had a remarkably close fit to the variation in area given by the JKR theory (figure 5), which

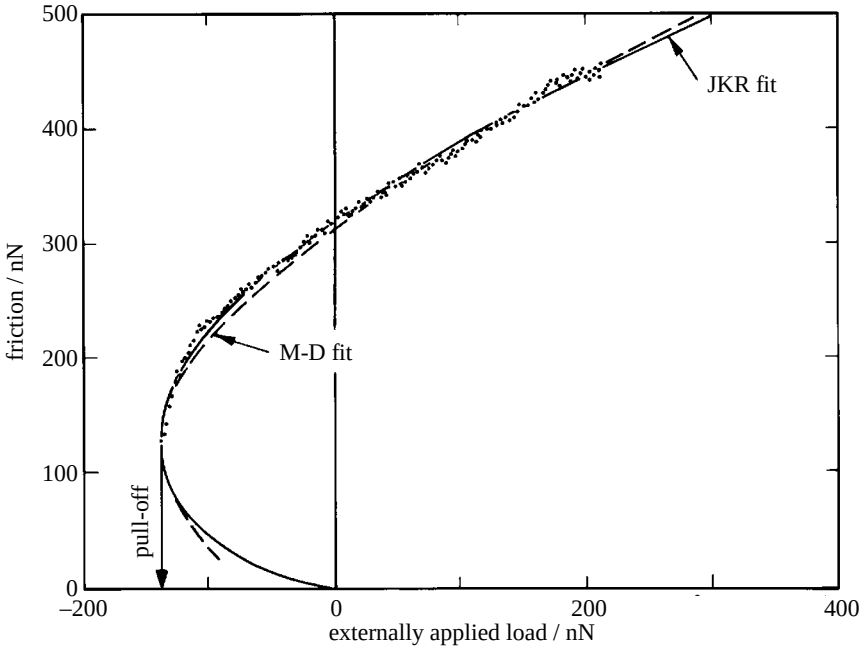

Figure 5. Friction measurements in UHV in the AFM (Carpick *et al.* 1996). Fitting the JKR area–load relationship gives $w = 0.21\ \mathrm{J\ m^{-2}}$ and a uniform frictional stress $\tau_0 = 0.84\ \mathrm{GPa}$. Fitting Maugis–Dugdale with $b = a + 0.4(c - a)$ gives $w = 0.19\ \mathrm{J\ m^{-2}}$ and $\tau_0 = 0.96\ \mathrm{GPa}$.

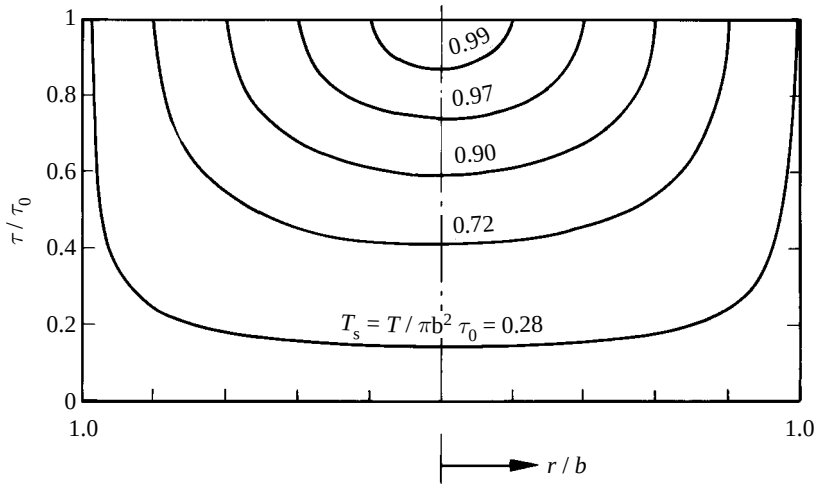

Figure 6. Traction distribution in static friction caused by the penetration of microslip from the periphery to the centre of the contact (equation (3.3)).

again strongly suggests a constant frictional shear stress. If it is assumed that this behaviour also applies in the microslip regime, before full sliding occurs, then we have the situation in mode II which is the equivalent of a 'Bilby–Cottrell–Swinden crack' in mode III, and of a Dugdale crack in mode I. The contact area comprises a central circle of radius e in which there is no slip, surrounded by an annulus ($e \leqslant r \leqslant b$) of microslip in which the shear traction τ_0 is constant. The traction distribution is continuous with no singularity at either $r = e$ or at $r = b$. It has been shown by

Savkoor (1987) to be

$$q(r) = \frac{\tau_0}{\pi} \arccos\left\{\frac{2b^2 - e^2 - r^2}{e^2 - r^2}\right\}, \quad r \leqslant e; \quad q(r) = \tau_0, \quad e \leqslant r \leqslant b \tag{3.3}$$

and is plotted in figure 6 for different values of $\gamma = e/b$. When $e \to b$, i.e. $\gamma \to 1$ this expression for the traction reduces to that in equation (3.1). The tangential force is expressed by

$$T = \int_0^b 2\pi q(r) r \, \mathrm{d}r = 2\tau_0 b^2 [\arccos\gamma + \gamma\sqrt{1-\gamma^2}] \tag{3.4}$$

and the tangential compliance by

$$D = \frac{(2-\nu)}{(1-\nu)E^*} \tau_0 b \sqrt{1-\gamma^2}. \tag{3.5}$$

The slip displacement s at $r = b$ when microslip has penetrated to $r = e = \gamma b$, has been found by Savkoor (1987) to be

$$s = \frac{2\tau_0 b}{(1-\nu)E^*} [(2-\nu)\{\sqrt{1-\gamma^2}\arccos\gamma + 1 - \gamma\} - \nu\cos 2\vartheta]. \tag{3.6}$$

Averaging round the periphery gives:

$$\bar{s} = \frac{2(2-\nu)\tau_0 b}{\pi(1-\nu)E^*} [\sqrt{1-\gamma^2}\arccos\gamma + 1 - \gamma]. \tag{3.7}$$

As the tangential force T is increased from zero to its limiting value $T_\mathrm{s} = \pi\tau_0 b^2$, microslip penetrates from the periphery to the centre (i.e. γ decreases from 1.0 to 0), and $\bar{s}$ increases from zero to a maximum $\bar{s}_\mathrm{s}$ according to equation (3.7). At this point complete sliding begins.

The question now arises: what is the radius b of the effective contact area over which the frictional traction acts? In the JKR regime the sharp edge of the contact makes b unequivocally equal to the JKR radius a, given by equation (2.15). In the Maugis–Dugdale regime the situation is far from clear cut. The surface separation increases in the Dugdale zone from zero at $r = a$ to h_0 at $r = c$, with a corresponding reduction in tangential surface force. Hence the effective radius b would be expected to lie between a and c. We write therefore

$$b = a + x(c - a), \tag{3.8}$$

where x is a factor between 0 and 1.

Returning to the AFM measurements in figure 5, Carpick *et al.* (1996) explain how the area πa^2, obtained from the JKR equation (2.15), was fitted to the friction measurements. Taking $E^* = 44$ GPa for a platinum tip of radius $R = 140$ nm in contact with mica, the JKR fit shown in figure 5 gives $w = 0.19\ \mathrm{J\,m^{-2}}$ and $\tau_0 = 0.84$ GPa. If the equilibrium z_0 separation is taken to be 0.2 nm, the above values give the Tabor elasticity parameter $\mu \approx 0.7$ or the Maugis–Dugdale parameter $\lambda \approx 0.8$. These values lie well in the Maugis regime, so that it is surprising at first sight that the measurements correlate so well with the JKR area. To resolve this paradox we note first that Greenwood (1996), in a numerical solution of the adhesion problem with a Lennard–Jones potential, defined the effective contact radius as that which coincided with the maximum in the Lennard–Jones force. He found that this radius agreed closely with the JKR radius for all values of μ greater than 0.5. In our case,

using the Maugis–Dugdale theory with $\lambda = 0.8$, taking $x = 0.4$ in equation (3.8) results in the area πb^2 having an equally good fit with the friction measurements in figure 5, yielding $w = 0.19$ and $\tau_0 = 0.96$ GPa.

We shall now consider the situation when friction specified by the above model is combined with the adhesion model specified in § 2.

4. Interaction between friction and adhesion

We now seek to model the possible interaction between friction and adhesion. In the conditions where linear elastic fracture mechanics (LEFM) applies, i.e. when the adhesion and slip zones are small compared with the contact radius, the situation is one of mixed mode interfacial fracture (see Hutchinson 1990). We can then express the strain energy release rate:

$$G = \frac{1}{2E^*}\left[K_{\mathrm{I}}^2 + K_{\mathrm{II}}^2 + \frac{1}{1-\nu}K_{\mathrm{III}}^2\right], \tag{4.1}$$

where K_{I}, K_{II} and K_{III} are given by equations (2.17) and (3.2). Averaging K_{II} and K_{III} round the periphery of the contact area simplifies equation (4.1) to

$$G = \frac{1}{2E^*}\left[K_{\mathrm{I}}^2 + \frac{2-\nu}{2-2\nu}K_{\mathrm{II}}^2\right]. \tag{4.2}$$

Fracture occurs when $G = G_c$, where G_c is the work of adhesion. We shall follow Hutchinson in writing

$$G_c = wf(K_{\mathrm{II}}/K_{\mathrm{I}}), \tag{4.3}$$

where, as previously, w is the work of adhesion in pure mode I loading. In the conditions of LEFM ($d \ll a$) the strain release energy release rate for a Dugdale crack in mode I is $\sigma_0 h_0$ and that for a BCS crack in mode II is $\tau_0 \bar{s}$ (Rice 1968), where $\bar{s}$ is the mean slip at $r = b$. Equation (4.3) may then be written:

$$\sigma_0' h_0 + \tau_0 \bar{s} = G_c = \sigma_0 h_0 f(\tau_0 \bar{s}/\sigma_0' h_0) = \sigma_0 h_0 f_1(\tau_0 \bar{s}/\sigma_0 h_0), \tag{4.4}$$

where it is assumed that the effect of friction is to reduce the Dugdale stress from σ_0 to σ_0', i.e. the work of adhesion from w to w'. Note that $\bar{s}$ is not constant, but increases with tangential force according to equations (3.4) and (3.7). Interaction with adhesion is unlikely to extend beyond a critical value of slip, denoted by $\bar{s}_0$, the magnitude of which is about one molecular spacing, i.e. comparable with h_0. We now, rather arbitrarily, choose the function f_1 to have the form

$$f_1(g) \equiv \sqrt{(1+g)^2 - 2\alpha g}, \tag{4.5}$$

where

$$g = (\tau_0 \bar{s}/\sigma_0 h_0), \quad \bar{s} \leqslant \bar{s}_0, \tag{4.6\,a}$$

or

$$g = g_0 = (\tau_0 \bar{s}/\sigma_0 h_0), \quad \bar{s} > \bar{s}_0, \tag{4.6\,b}$$

and α is a non-dimensional interaction factor.

We note in passing that the theory of interaction proposed by Savkoor & Briggs (1977) takes G to be given by equation (4.2) and G_c to be given by equation (4.3) in which $f(K_{\mathrm{II}}/K_I)$ *is taken to be unity*. This assumption corresponds to an 'ideally

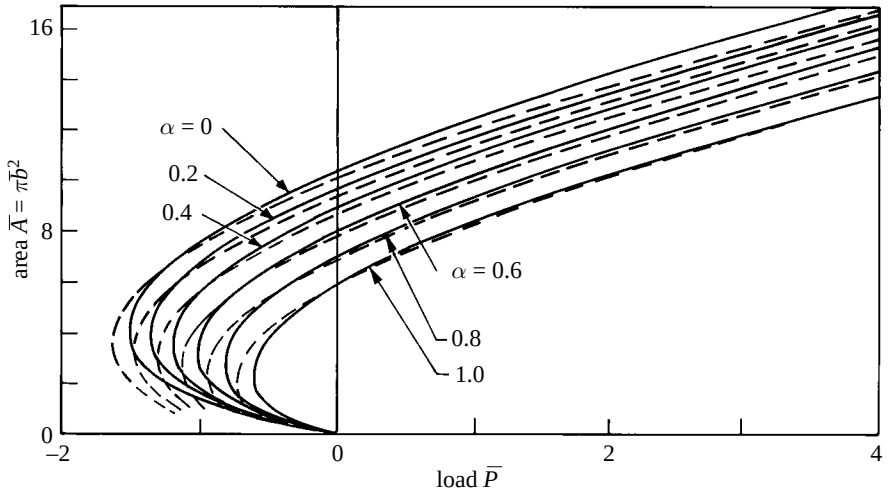

Figure 7. Effect of the interaction factor α on the area–load curves: ——, JKR; – – –, Maugis–Dugdale ($\lambda = 0.8$, $\tau_0 = 0.96$ GPa). $(\bar{P}_c)_{\text{sliding}}/(\bar{P}_c)_{\text{static}} = 0.89$ gives $\alpha \approx 0.2$.

brittle' fracture in which frictional energy dissipation is neglected. For $f_1(g) = 1$, $\alpha = 1 + \frac{1}{2}g$.

For small values of λ or when the slip zone is no longer small, the quantities can only be identified approximately as the strain energy release rates (Kim *et al.* 1996). Nevertheless, equations (4.4)–(4.6) will still be taken to govern the interaction between adhesion and friction. Equation (4.4) then gives

$$X \equiv \frac{w'}{w} = \frac{\sigma_0'}{\sigma_0} = \sqrt{(1+g)^2 - 2\alpha g - g}. \tag{4.7}$$

The influence of friction on the Maugis–Dugdale model of adhesion can now be found by replacing σ_0 by σ_0' in equations (2.7) and (2.9), so that equations (2.12) and (2.13) become

$$\tfrac{1}{2}X\lambda\bar{a}^2\{(m^2-2)\arccos(1/m)+\sqrt{m^2-1}\}+\tfrac{4}{3}\lambda^2\bar{a}\{\sqrt{m^2-1}\arccos(1/m)-m+1\} = 1 \tag{4.8}$$

and

$$\bar{P} = \bar{P}_1 + \bar{P}_{\text{a}} = \bar{a}^3 - X\lambda\bar{a}^2\{\sqrt{m^2-1} + m^2\arccos(1/m)\}. \tag{4.9}$$

For any given values of λ, g and interaction parameter α, equations (4.7)–(4.9) can be solved simultaneously to find $\bar{a}$ and $\bar{c}$ as a function of the load $\bar{P}$. The contact area $\bar{A} = \pi b^2$ is found from equation (3.8) (with $x = 0.4$) and plotted against $\bar{P}$ in figure 7 (shown dotted).

If $\lambda > 5$, adhesion is governed by the JKR theory. The interactive effect of friction can then be found by replacing w by w' in equation (2.15), with the result

$$\bar{P} = \bar{a}^3 - \sqrt{6X\bar{a}^3} = \bar{P}_1 - \sqrt{6X\bar{P}_1} = (\bar{A}/\pi)^{3/2} - \sqrt{6X(\bar{A}/\pi)^{3/2}}, \tag{4.10}$$

where X is given by equation (4.7). In these circumstances the contact radius $b = a$. The corresponding area–load curves obtained from equation (4.10) are also plotted in figure 7 (full lines). Note that defining the contact size by equation (3.8) makes the difference between the Maugis–Dugdale and JKR estimates of contact area small for all values of λ greater than 0.3.

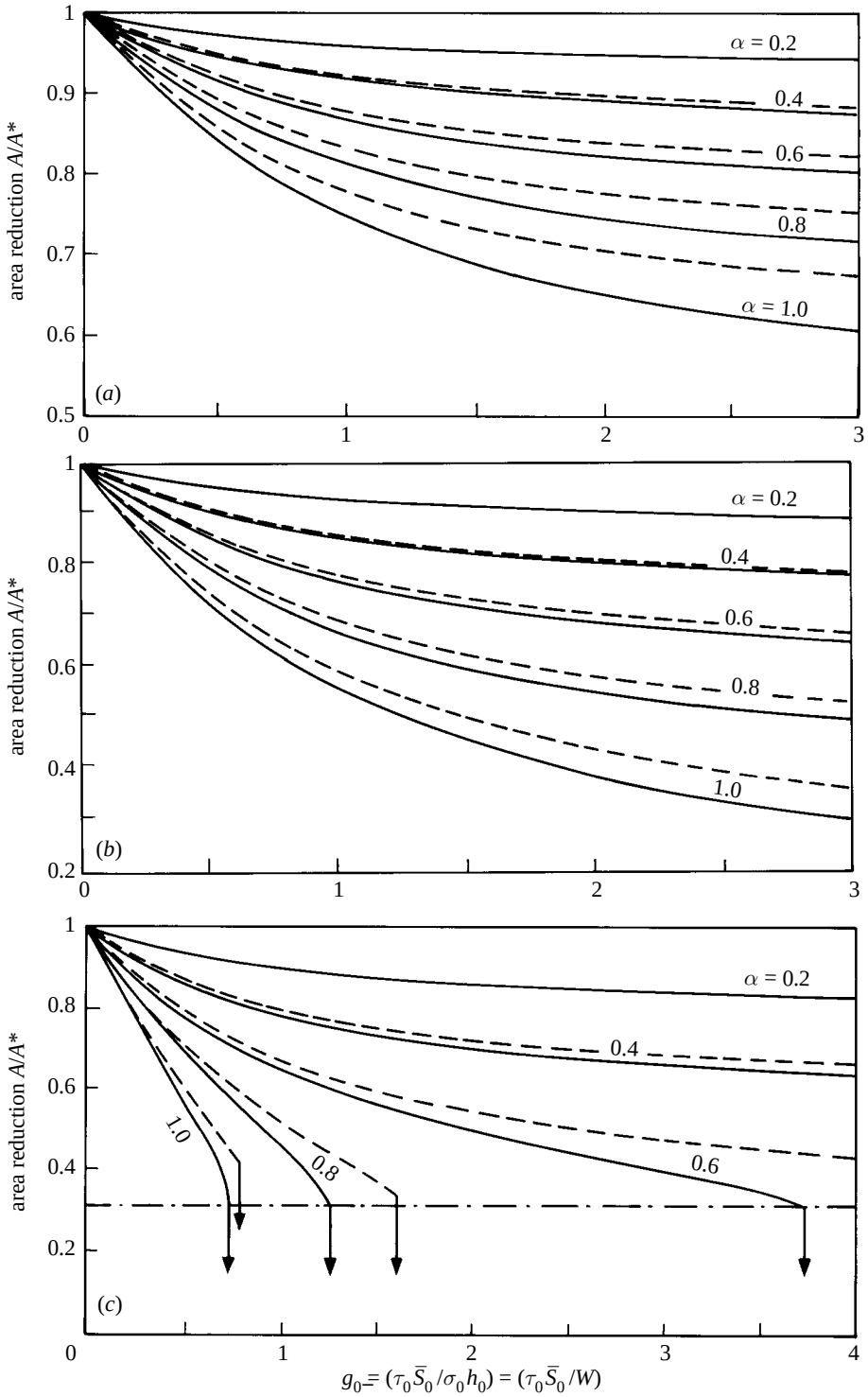

Figure 8. Effect of shear traction on the contact area during sliding: ——, JKR; – – –, Maugis–Dugdale ($\lambda = 0.8$). (*a*) $\bar{P} = 3.0$, (*b*) $\bar{P} = 0$, (*c*) $\bar{P} = -0.75$.

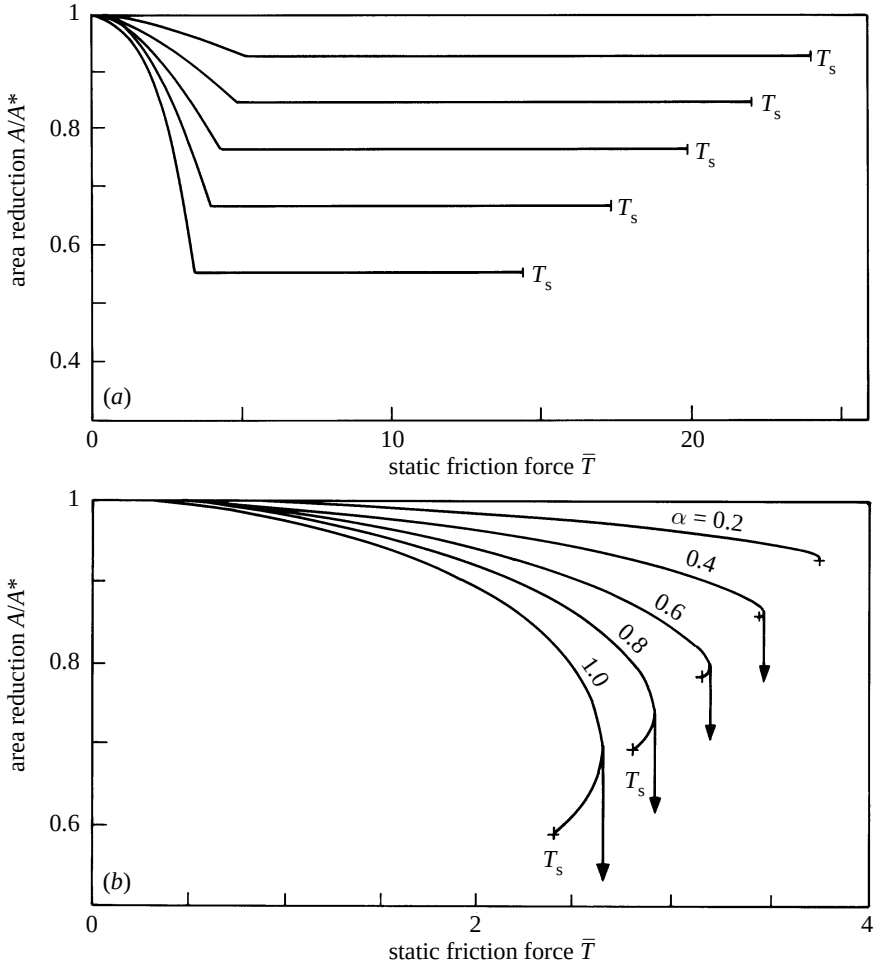

Figure 9. Peeling of the contact area during the static friction phase $T < T_s(= \pi b^2 \tau_0)$; $\bar{P} = 0$. (*a*) $\lambda = 5$ (JKR), $g_0 = 1$, $\tau_0 = 5$. (*b*) $\lambda = 0.8$ (M–D), $g_0 = 1$, $\bar{\tau}_0 = 0.8$.

(*a*) *Complete sliding*

During sliding motion the slip $\bar{s}$ at the edge of the contact will exceed the critical value $\bar{s}_0$ so that g will take the constant value $g_0 = (\tau_0 \bar{s}_0 / \sigma_0 h_0)$ prescribed by equation (4.6 *b*). The non-dimensional contact radius and area in the absence of any interaction ($\alpha = 0$) are denoted by $\bar{b}^*$ and $\bar{A}^*$. At any given load $\bar{P}$ the effect of interaction is to cause a reduction in adhesion and hence a decrease in the contact size. In the Maugis–Dugdale regime ($\lambda < 5$) the reduction in area $\bar{A}/\bar{A}^*$ is calculated as a function of g_0 and α from equations (3.8), (4.7) and (4.10). By way of example, the reduction in area for $\lambda = 0.8$ (corresponding to the experimental results in figure 5) is plotted for loads $\bar{P} = 3$, 0 and -0.75 in figures 9 (shown dotted). Comparative results for the JKR regime ($\lambda > 5$), obtained from equations (4.7) and (4.10), are also included in figure 9 (full lines). It is clear from this example that the reduction in adhesion brought about by sliding is not very different in the two regimes.

As the experiments have shown, sliding contact is possible with negative loads, but the analysis shows that this can only be achieved if the degree of interaction is

limited. For equation (4.10) to have a real solution $X \geqslant -\frac{2}{3}\bar{P}$, whereupon $\bar{a}^3 \geqslant -\bar{P}$. If the contact size attempts to fall below this critical value, the surfaces snap apart, as shown in figure 8*c* when α exceeds 0.5. As mentioned previously, the Savkoor & Briggs (1977) interaction model corresponds to a value of $\alpha = 1 + \frac{1}{2}g$ and therefore predicts that sliding at negative loads is impossible.

(*b*) *Static friction*

As a tangential force T applied to the contact is increased from zero to its limiting value $T_s = \pi\tau_0 b^2$, microslip spreads through the interface from the periphery according to equations (3.4) and (3.7). Increasing slip $\bar{s}$ at the periphery reduces the adhesion by equations (4.6*a*) and (4.7), with a consequent reduction in contact size, until the critical slip $\bar{s}_0$ is reached. The sequence of events during the static friction stage can take two forms. Where the parameter λ is large (JKR regime), the critical slip $\bar{s}_0$ is reached *before* the onset of sliding. No further reduction in contact size then takes place up to, and through, the point of sliding, as illustrated in figure 9*a*. Alternatively, with lower values of λ the contact can be on the point of sliding before the critical slip is reached. However, as soon as sliding begins, the critical slip will be reached and the contact size will drop to its final value, as illustrated in figure 9b.

A feature of note in figure 9b, at larger values of the interaction parameter α, is a maximum in the tangential force in excess of the limiting friction force. In a system which is purely 'force controlled' this feature would lead to unstable accelerated sliding. However, both the SFA and AFM apply the tangential force through a spring. In these circumstances the onset of sliding would be accompanied by a 'jump' in displacement, with the probability of stick–slip motion.

5. Discussion and comparison with experiments

In conditions where it is appropriate ($\lambda > 5$, say) the JKR theory of straight adhesion outlined in § 1 has received exhaustive experimental support and will not be discussed further here. Static friction measurements under adhesive conditions have been made on soft rubber by Savkoor & Briggs (1977) and Barquins (1985). Sliding friction has been measured between polymer monofilaments at negative (adhesive) loads by Briscoe & Kremnitzer (1979), between mica surfaces in the SFA by Israelachvili (1992) (figure 4) and between a platinum coated ceramic tip and mica in the AFM by Carpick *et al.* (figure 5)†.

Savkoor & Briggs (1977) applied a monotonically increasing tangential force to a rubber hemisphere in adhesive contact with a clean glass plate, for a series of normal loads. They observed that the contact size decreased progressively as shown in figure 10. They also presented an analysis which has much in common with the present approach. The strain energy release rate was given by equation (4.2), but the total work of adhesion was assumed to be w, ignoring energy dissipated by friction. The analysis predicted a critical tangential force at which the contact area would collapse to the Hertzian value, as indicated in figure 10, above which sliding contact would not be possible with a negative load.

The Savkoor & Briggs analysis and an earlier treatment by the present author

† Difficulties in accurate calibration of the dynamometer springs could be responsible for a *consistent* error in the load and friction force in figure 5 by up to a factor of two, but the *shape* of the curve would be unaffected.

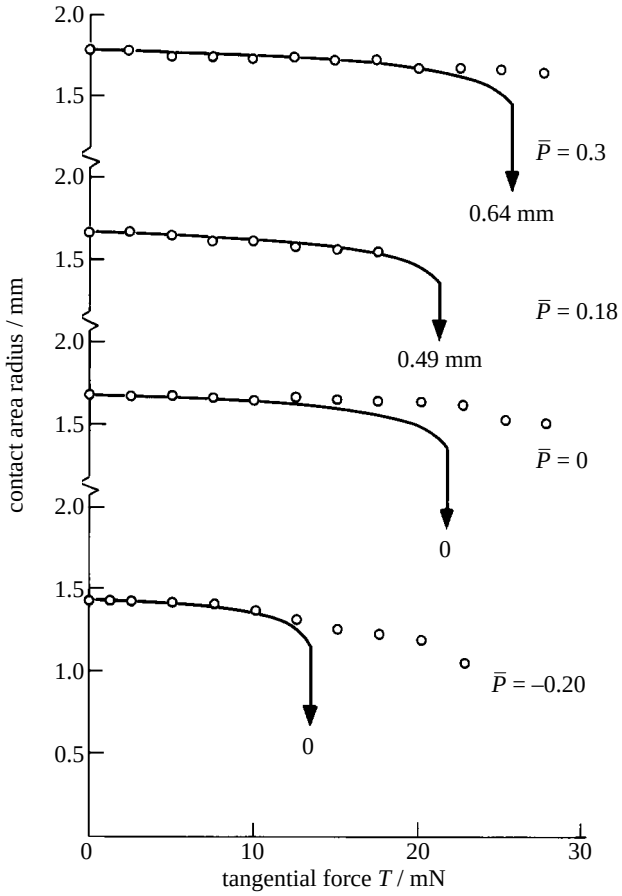

Figure 10. Contact area measurements during the static friction phase, made with a soft rubber hemisphere in contact with a glass plate, from Savkoor & Briggs (1977). ○, experimental; ——, S & B theory.

(Johnson 1996) raise the question of the appropriate model for the mode II 'interface crack': *either* in terms of a stress intensity K_{II}, *or* as a BCS crack with no discontinuity in traction, as adopted in § 3. Rice (1992) has modelled the nucleation of glide dislocations from the tip of a mode II crack through the action of a stress intensity K_{II}, with the result that the tangential driving force T is proportional to the contact size $a^{3/2}$. The experimental evidence from the SFA and AFM in figures 4 and 5, on the other hand, shows the sliding friction force to be proportional to a^2. This strongly suggests that the principal contribution to the force of sliding friction comes from propagating dislocations through the whole area of the interface, i.e. the effective Peierls stress, rather than from nucleation at the periphery. This is consistent with the BCS model of a mode II crack in the static friction phase. Propagation of dislocations along a glide plane in a regular crystal lattice is an oversimple model of sliding at a non-commensurate interface, but it is worth noting that an approximate value for the Peierls stress is quoted by Cottrell (1953) to be $2^{-4} \times$ (shear modulus), which for mica gives $7 \times 10^6\ \mathrm{N\,m^{-2}}$, the same order as the frictional stress of $2 \times 10^7\ \mathrm{N\,m^{-2}}$ measured by Israelachvili (1992). To summarize, it is recognized that periodic fluctuations in tangential stress will occur *on the atomic*

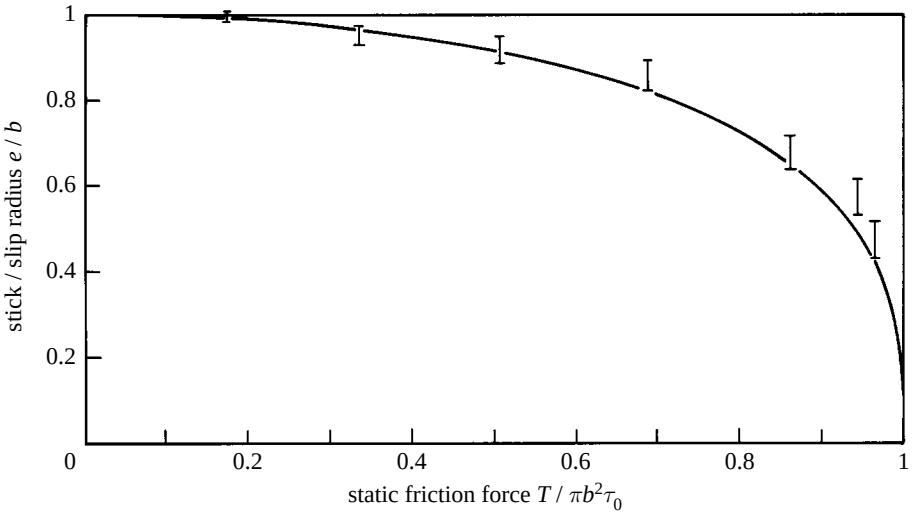

Figure 11. Measurements of the penetration of microslip between a soft rubber sphere and glass compared with the model of § 3 (equations (3.4) and (3.7).

scale as the equivalent of dislocations are nucleated at the periphery of the contact and propagated through the contact area, but our continuum theory smooths out these fluctuations, giving rise to the steady continuous distribution of traction expressed by equation (3.3).

Further support for the static friction phase of the model proposed in § 3 is provided by experiments of Barquins *et al.* (1975) with a glass sphere in contact with a smooth flat surface of natural rubber. The penetration of the microslip zone with increasing tangential force was observed and found to agree well with that predicted by equation (3.4), as shown in figure 11.

Reduction in adhesion leads to the surfaces peeling apart at the edges of the contact. As already mentioned, experimenting with rubber, Savkoor & Briggs observed a modest amount of peeling (figure 10) as did Barquins *et al.* (1975). On the other hand, in the SFA, Israelachvili (personal communication) did not see any change in the contact size when a tangential force was applied†. In the AFM experiments by Carpick *et al.* (1996) (figure 5), the contact size could not be measured. However, the pull-off force P_c in straight adhesion was measured before and after a sliding experiment, and compared with the force at which contact was lost in sliding. For the results shown in figure 5 the ratio was 0.89. The dotted curves in figure 7 show the effect of interaction on the Maugis–Dugdale area–load relationship for the conditions of figure 5, from which it may be seen that a 0.89 reduction in the pull-off force corresponds to a value of $\alpha \approx 0.2$.

The physical nature of this interaction between adhesion and friction can only be speculated upon, but it must arise from the interactive nature of the surface force field at the periphery of the contact in the presence of both normal and tangential displacements. It would be likely to manifest itself by an increased separation of

† The contact mechanics in this paper, as in Hertz and JKR, is based on homogeneous half-space theory, but the SFA consists of thin sheets of high-modulus material attached to a low-modulus glue. The possible effects of this construction on the contact mechanics of the adhesion theory is currently being investigated.

the surfaces during sliding compared with a static contact. We have shown how α, as a measure of interaction, might be found experimentally; perhaps molecular dynamics might throw light on the physical process. It will be appreciated that, in this model, adhesion and its interaction with friction is governed by surface forces at the *periphery* of the contact. The frictional resistance to sliding, on the other hand, is the integrated effect of proagating 'dislocations' throughout the whole contact area.

Given a value of α, to estimate the effect on the contact area during sliding requires a value for the parameter $g_0 = (\tau_0 \bar{s}_0/\sigma_0 h_0) = (\tau_0 \bar{s}_0/w)$. The quantity $\tau_0 \bar{s}_0$ is comparable with the 'unstable stacking fault energy' employed by Rice (1992) in his analysis of dislocation nucleation at the tip of a mode II crack. The tangential displacement (microslip) at the periphery $\bar{s}_0$, which gives rise to the interaction with adhesive forces is not precisely prescribed. It is likely to be the order of half an atomic spacing. In the calculations shown in figures 8 and 9 we have taken $\bar{s}_0 = h_0 = 0.2$ nm. On this basis, for the AFM measurements in figure 5, $g_0 \approx 1.0$, $\alpha = 0.2$ and $\lambda = 0.8$, whereupon the reduction in area A/A^* is by a factor of about 0.93. For the SFA measurements in figure 4, $g \approx 0.08$, so that the predicted reduction in area is only a few percent, which would account for it not being observed.

The model presented in this paper was developed for dry, clean, solid surfaces in contact, but it would appear to be applicable in principle to surfaces separated by nanometre films of lubricant, where Israelachvili (1992) has shown that adhesion can still be a significant effect. However, viscous dissipation in the film introduces a further complication: 'adhesion hysteresis', in which the work of adhesion in separating the surfaces is greater than that which is returned when they are coming together. In separation the elastic energy release has to overcome the viscous dissipation as well as the surface energy; in coming together it is the surface energy which has to provide for the dissipation in addition to increasing the elastic strain energy. Similar behaviour is found in the adhesion of dry rubber surfaces in response to the viscoelastic property of the rubber (see Greenwood & Johnson 1981). The influence of *inelastic* effects either in the film or in the deforming solids lies beyond the scope of this paper.

In conclusion it may be stated that a continuum mechanics model of adhesion and friction between smooth clean spherical elastic surfaces has been presented which is consistent with available experimental data. It is based on the concepts of fracture mechanics and incorporates possible interaction between normal adhesive forces and tangential friction forces. The transition from static to sliding friction is included. Being a continuum theory force fluctuations at the atomic scale are smoothed out; nevertheless it is hoped that the model will provide a rational and quantitative framework for the analysis and interpretation of experimental data in the rapidly expanding field of nanotribology.

I acknowledge the constructive discussions of the draft of this paper with many colleagues and, in particular, Professor S. Y. Kim and Professor R. McMeeking for their analysis of the strain energy release rate in axisymmetric cracks.

References

Arvanitaki, A., Briscoe, B. J., Adams, M. J. & Johnson, S. A. 1994 *Proc. 21st Leeds–Lyon Symposium on Tribology* (ed. C. M. Taylor). New York: Elsevier.

Barquins, M., Maugis, D. & Courlel, R. 1975 Micro-glissements dans l'aire de contact d'une bille de verre et d'une plaque de caoutchouc. *C. R. Acad. Sci., Paris* B **280**, 49–52.

Bowden, F. P. & Tabor, D. 1950 *Friction and lubrication of solids*. Oxford University Press.

Bradley, R. S. 1932 The cohesive force between solid surfaces and the surface energy of solids. *Phil. Mag.* **13**, 853–862.

Briscoe, B. J. & Kremnitzer, S. L. 1979 A study of the friction and adhesion of polyethyleneterephthalate monofilaments. *J. Phys.* D **12**, 505–516.

Carpick, R. W., Agrait, N., Ogletree, D. F. & Salmeron, M. 1996 Variation of the interfacial shear strength and adhesion of a nanometer sized contact. *Langmuir* **12**, 3334–3340.

Cotterell, A. H. 1953 *Dislocations and plastic flow in crystals*. Oxford University Press.

Derjaguin, B. V., Muller, V. M. & Toporov, Y. P. 1975 Effect of contact deformations on the adhesion of particles. *J. Colloid Interface Sci.* **67**, 378–326.

Dugdale, D. S. 1960 Yielding of steel sheets containing slits. *J. Mech. Phys. Solids* **8**, 100.

Greenwood, J. A. 1997 Adhesion of elastic spheres. *Proc. R. Soc. Lond.* A **453**. (In the press.)

Greenwood, J. A. & Johnson, K. L. 1981 The mechanics of adhesion of viscoelastic solids. *Phil. Mag.* A **43**, 697.

Homola, A. M., Israelachvili, J. N., McGuiggan, P. M. & Hellgeth, J. W. 1990 Fundamental studies in tribology. *Wear* **136**, 65–84.

Hutchinson, J. W. 1990 Mixed mode fracture mechanics of interfaces. In *Metal–ceramic interfaces* (ed. M. Ruhle *et al.*). New York: Pergammon.

Israelachvili, J. 1992 Adhesion, friction and lubrication of molecularly smooth surfaces. In *Fundamentals of friction* (eds I. L. Singer & H. M. Pollock), NATO ASI Series E, vol. 220, p. 351.

Johnson, K. L. 1985 *Contact mechanics*. Cambridge University Press.

Johnson, K. L. 1996 Continuum mechanics modelling of adhesion and friction. *Langmuir* **12**, 4510–4513.

Johnson, K. L., Kendall, K. & Roberts, A. D. 1971 Surface energy and the contact of elastic solids. *Proc. R. Soc. Lond.* A **324**, 301–313.

Maugis, D. 1992 Adhesion of spheres: the JKR–DMT transition using a Dugdale model. *J. Colloid Interface Sci.* **150**, 243–269.

Maugis, D. & Barquins, M. 1978 Fracture mechanics and the adherance of viscoelastic bodies. *J. Phys.* D **11**, 1989.

Muller, V. M., Yushenko, V. S. & Derjaguin, B. V. 1980 On the influence of molecular forces on the deformation of an elastic sphere and its sticking to a rigid plane. *J. Colloid Interface Sci.* **77**, 91–101.

Muller, V. M., Yushenko, V. S. & Derjaguin, B. V. 1983 *Coll. Surf.* **7**, 251–259.

Pashley, M. D. 1984 Further consideration of the DMT model for elastic contact. *Coll. Surf.* **12**, 69–77.

Rice, J. R. 1968 A path indepedent integral and the approximate analysis of strain concentration by notches and cracks. *J. Appl. Mech. Trans. ASME* **90**, 379.

Rice, J. R. 1992 Dislocation nucleation from a crack tip: an analysis based on the Peierls concept. *J. Mech. Phys. Solids* **40**, 239–272.

Sarid, D. 1991 *Scanning force microscopy: with applications to electric, magnetic and atomic forces*. Oxford University Press.

Savkoor, A. R. 1987 *Dry adhesive contact of elastomers*. M.Engng dissertation, Tech. University, Delft, Netherlands.

Savkoor, A. R. & Briggs, G. A. D. 1977 The effect of a tangential force on the contact of elastic solids in adhesion. *Proc. R. Soc. Lond.* A **356**, 103–114.

Tabor, D. 1976 Surface forces and surface interactions. *J. Colloid Interface Sci.* **58**, 1–13.

Received 6 February 1996; revised 14 June 1996; accepted 26 July 1996